

INSTRUMENTS AND METHODS OF INVESTIGATION

PACS numbers: 07.79.Fc, **41.20. – q**, 68.37.Vj

The near-field microscope as a tool for studying nanoparticles

I S Osad'ko

DOI: 10.3367/UFNe.0180.201001c.0083

Contents

Abstract. The oscillating electric dipole field induced by laser light at the probe tip of the near-field microscope is shown to allow a higher resolution compared to the conventional optical microscope.

1. Introduction

The invention of various types of probe microscopes has provided researchers with new nanometer-resolution tools for probing molecules on a surface [1]. The probe — the key to the concept — is a thin needle made either of metal (as in tunneling microscopes, where the current between the needle and the substrate is measured) or of an optically transparent insulating material (as in the scanning near-field optical microscopes, SNOMs [2], which use light to excite molecules on the surface).

It is well known that conventional and electron microscopes (respectively using light and electrons as a 'probe') cannot resolve two objects separated by less than the wavelength of light λ and the de Broglie electron wavelength. That light-based SNOMs discern objects only a few hundredths of λ apart seems quite bizarre from the standpoint of traditional wave microscopy. The present article gives an undergraduate-oriented explanation of why the SNOM has a resolving power tens of times exceeding that of its optical counterparts.

Qualitatively, the answer is simple and is well illustrated in Fig. 1. Light, e.g., from a blue laser is directed via a light guide to a quartz needle coated by metal everywhere except the tip, the tip diameter being less than the wavelength of light. The polarization thereby induced in the free tip oscillates at the laser frequency and produces an alternating electromagnetic field outside the needle, a complex superposition of electric and magnetic multipoles. Of these, as we show in Section 4, the alternating electric field of the induced dipole is strongest near the tip. Because this field decreases with r as $1/r^3$, molecules far away from the needle are excited by it much less than those located near it, in the so-called near zone, a region whose size is much less than the wavelength of the light passing through the needle.

The excited molecules of the substrate fluoresce, and their radiation is detected by a photomultiplier tube (PMT). Because the fluorescence intensity of a molecule is proportional to the molecule excitation probability and because this probability is greatest for molecules in the near zone, precisely these molecules contribute most to the fluorescence signal; the fluorescence from molecules outside the near zone is lost in the photoreceiver noise. In Fig. 1, the arrows directed to the PMT are given different thicknesses to illustrate that molecules fluoresce with different intensities due to their different excitation energies. When moving the needle along the surface under study, the fluorescence signal at any moment is mainly due to the molecules that are precisely beneath the needle, i.e., in the near zone, at this moment. Hence, moving the tip along the surface of the sample means scanning the surface with a resolution better than the exciting wavelength. In what follows, we take a closer look at the physics behind this phenomenon.

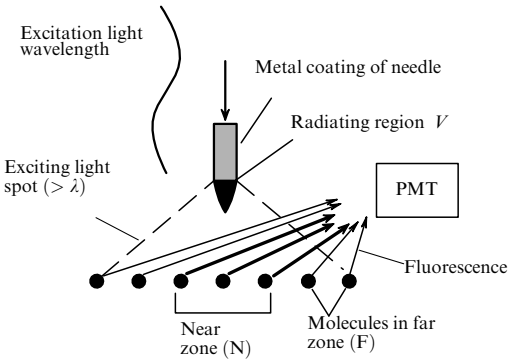

Figure 1. Principle of near-field microscope.

I S Osad'ko Lebedev Physical Institute, Russian Academy of Sciences, Leninskii prosp. 53, 119991 Moscow, Russian Federation
Tel. (7-499) 135 78 91
E-mail: osadko@sci.ledebev.ru

Received 24 April 2009, revised 13 September 2009
Uspekhi Fizicheskikh Nauk **180** (1) 83 – 87 (2010)
DOI: 10.3367/UFNr.0180.201001c.0083
Translated by E G Strel'chenko; edited by A M Semikhatov

2. Near and far zones

The first thing we need to do is to estimate the distribution of the electromagnetic field in the SNOM. This is a rather complex mathematical physics problem; it is solvable for some specific probe models, but as regards the explanation of the resolving power of the SNOM, a certain simplifying assumption can be made and, in addition, the existence of characteristic scales and of the associated small parameters can be used.

The schematic diagram in Fig. 2 shows the radiating region V of size L, which models the probe tip; the exciting light wave; and the near and far (relative to V) wave zones with their respective characteristic scales. The region V features the oscillating charge density ρ and the current density $\mathbf{j}$, both induced by the exciting laser radiation and acting together as a source of the electromagnetic field for the exterior of region V. In near-field spectroscopy, the terms near and far are very naturally used for the fields respectively dominating in the near and far zones.

The assumption mentioned above is that in the region filled with the molecules under study, the probe and light-guide boundary effects can be neglected and the electromagnetic field can therefore be calculated using the well-known vacuum expressions for the retarded potentials due to the charges and currents in V. In the Lorentz gauge, the corresponding expressions for the scalar and vector potentials are [3]

$$\varphi(\mathbf{r},t)=\int_V \frac{\rho(\mathbf{r}',t-R/c)}{R}\,\mathrm{d}V',$$
$$\mathbf{A}(\mathbf{r},t)=\frac{1}{c}\int_V \frac{\mathbf{j}(\mathbf{r}',t-R/c)}{R}\,\mathrm{d}V', \tag{1}$$

where $R=|\mathbf{r}-\mathbf{r}'|=\sqrt{r^2+r'^2-2(\mathbf{r}\mathbf{r}')}$ and the meaning of the radius vectors is made clear in Fig. 3.

The electric and magnetic vectors are to be found from the well-known field–potential relations

$$\mathbf{E}=-\nabla\varphi-\frac{\dot{\mathbf{A}}}{c},\quad \mathbf{B}=[\nabla\mathbf{A}]. \tag{2}$$

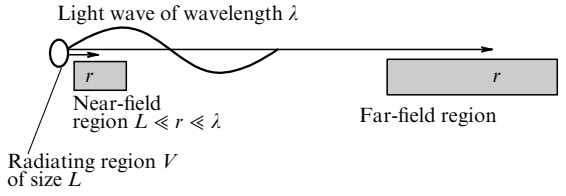

Figure 2. Radiating volume, near zone, and far zone (schematic).

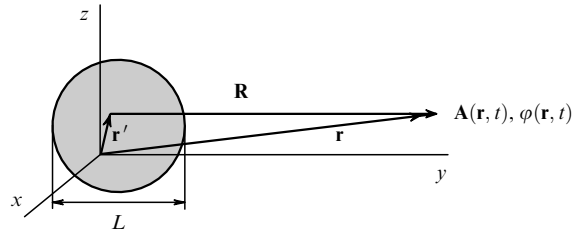

Figure 3. Radiating region V, the radius vector $\mathbf{r}$ to the point of observation, and the radius vector $\mathbf{r}'$ to a point in V.

The expressions for the fields we derive below are the leading terms in their expansion in the small parameters

$$\frac{L}{r}\ll 1,\quad \frac{2\pi L}{\lambda}\ll 1. \tag{3}$$

According to Fig. 2, these inequalities are satisfied for the near zone and even more so for the far zone. The corresponding expressions are obtained by expanding the integrands in Eqn (1) in the respective small parameters

$$\frac{r'}{r}\leqslant\frac{L}{r}\ll 1,\quad \frac{2\pi r'}{\lambda}\leqslant\frac{2\pi L}{\lambda}\ll 1. \tag{3a}$$

The meaning of the second parameter can be clarified by introducing the retardation time $t_\mathrm{r}=r/c$ (for a signal traveling from region V to the point of observation) and the self-retardation time $t'_\mathrm{r}=r'/c$ (the retardation time difference for signals coming from different points in V).

With ω denoting the frequency of the light exciting molecules on the surface (which is also the oscillation frequency of the charge density ρ and current density $\mathbf{j}$), conditions (3a) can be written in the equivalent form

$$\frac{r'}{r}\ll 1,\quad t'_\mathrm{r}\omega\ll 1. \tag{3b}$$

The small value of the second parameter implies that the self-retardation is small compared to the light wave period.

3. Small-parameter expansion of the potentials

We consider the two functions in the integrand in the expression for the scalar potential. Expanding them to the first order in small parameters (3a) and (3b), we obtain

$$\frac{1}{|\mathbf{r}-\mathbf{r}'|}\cong\frac{1}{r}+\frac{(\mathbf{r}'\mathbf{n})}{r^2},$$
$$\rho\left(\mathbf{r}',t-\frac{R}{c}\right)\cong\rho\left(\mathbf{r}',\tau+\frac{(\mathbf{r}'\mathbf{n})}{c}\right)$$
$$\cong\rho(\mathbf{r}',\tau)+\frac{\partial\rho(\mathbf{r}',\tau)}{\partial\tau}\,\frac{(\mathbf{r}'\mathbf{n})}{c}, \tag{4}$$

where $\tau=t-r/c=t-t_\mathrm{r}$ and $\mathbf{n}=\mathbf{r}/r$ is the unit vector. It is clear that

$$\frac{\partial\rho(\mathbf{r}',\tau)}{\partial\tau}\,\frac{(\mathbf{r}'\mathbf{n})}{c}\cong\rho\omega t'_\mathrm{r}\ll\rho$$

is indeed linear in the small parameter. Substituting expansions (4) in the formula for the scalar potential yields

$$\varphi(\mathbf{r},t)\cong\int_V\left(\frac{1}{r}+\frac{(\mathbf{r}'\mathbf{n})}{r^2}\right)\left(\rho(\mathbf{r}',\tau)+\dot{\rho}(\mathbf{r}',\tau)\,\frac{(\mathbf{r}'\mathbf{n})}{c}\right)\mathrm{d}V'. \tag{5}$$

With the term proportional to the product of the two small parameters neglected, this becomes

$$\varphi(\mathbf{r},t)\cong\varphi_\mathrm{m}(r,\tau)+\varphi_\mathrm{d}(\mathbf{r},\tau)+\varphi_\mathrm{rad}(\mathbf{r},\tau), \tag{6}$$

where

$$\varphi_\mathrm{m}(r,\tau)=\frac{1}{r}\int_V\rho(\mathbf{r}',\tau)\,\mathrm{d}V'=\frac{e(\tau)}{r} \tag{6a}$$

is the Coulomb potential of the total charge of the system, $e(\tau)$. In our case, region V is electrically neutral, and hence this charge is zero. The second term,

$$\varphi_{\rm d}(\mathbf{r},\tau)=\frac{1}{r^2}\int_V(\mathbf{r}'\mathbf{n})\,\rho(\mathbf{r}',\tau)\,{\rm d}V'=\frac{\big(\mathbf{d}(\tau)\,\mathbf{n}\big)}{r^2}\,, \tag{6b}$$

is the potential of the total dipole of the system, $\mathbf{d}(\tau)$. Finally,

$$\varphi_{\rm rad}(\mathbf{r},\tau)=\frac{1}{r}\int_V\dot\rho(\mathbf{r}',\tau)\,\frac{(\mathbf{r}'\mathbf{n})}{c}\,{\rm d}V'=\frac{\big(\dot{\mathbf{d}}(\tau)\,\mathbf{n}\big)}{cr} \tag{6c}$$

is the scalar potential of the radiation.

The expansion of the scalar potential in powers of the small parameter L/r is the multipole expansion, $\varphi_{\rm m}$ and $\varphi_{\rm d}$ being the monopole and dipole potentials none of which vanishes even for a static charge distribution $\rho(\mathbf{r}')$ in region V. The radiation potential $\varphi_{\rm rad}$ is linear in the small parameter $t'_{\rm r}\omega$; $\varphi_{\rm rad}$ is due to the alternating dipole moment.

We take the vector potential to be given by the first nonvanishing term in the expansion of the integrand in powers of small parameters (3a) and (3b):

$$\begin{aligned}\mathbf{A}(\mathbf{r},t)&=\frac{1}{c}\int_V\frac{\mathbf{j}(\mathbf{r}',t-R/c)}{R}\,{\rm d}V'\cong\frac{1}{cr}\int_V\mathbf{j}(\mathbf{r}',\tau)\,{\rm d}V'\\&=\frac{1}{cr}\int_V\sum_i e_i\mathbf{v}_i(\tau)\,\delta(\mathbf{r}'-\mathbf{r}_i)\,{\rm d}V'\\&=\frac{1}{cr}\sum_i e_i\mathbf{v}_i(\tau)=\frac{\dot{\mathbf{d}}(\tau)}{cr}=\mathbf{A}_{\rm rad}(\mathbf{r},t)\,,\end{aligned} \tag{7}$$

where the coordinate $\mathbf{r}_i$ indicates the location of charges in V. The scalar and vector potentials are related by the simple formulas

$$\mathbf{A}_{\rm rad}(\mathbf{r},\tau)=\frac{\dot{\mathbf{d}}(\tau)}{cr}\,,\quad\varphi_{\rm rad}(\mathbf{r},\tau)=\big(\mathbf{n}\mathbf{A}_{\rm rad}(\mathbf{r},\tau)\big)\,. \tag{8}$$

It follows that expanding retarded potentials (1) in powers of small parameters (3) results in the potentials expressed in terms of the electric dipole moment of region V in the first nonvanishing approximation.

4. Far and near fields

Having obtained rather simple formulas (6) and (7) for the scalar and vector potentials, we can substitute them in Eqns (2) to find the electric and magnetic fields. The procedure is as follows.

First, substituting Eqn (7) in the magnetic field expression and noting that the operator ∇ differentiates $d(\tau)$ with respect to time and multiplies it by $-\mathbf{n}/c$, i.e.,

$$\boldsymbol{\nabla}\,d(\tau)=-\frac{\mathbf{n}}{c}\,\frac{\partial}{\partial\tau}\,d(\tau)\,, \tag{9}$$

we arrive at the following expression for the magnetic field:

$$\mathbf{B}=\frac{1}{cr}\big[\boldsymbol{\nabla}\,\dot{\mathbf{d}}(\tau)\big]-\left[\dot{\mathbf{d}}(\tau)\,\boldsymbol{\nabla}\,\frac{1}{cr}\right]=\frac{[\ddot{\mathbf{d}}\mathbf{n}]}{c^2r}+\frac{[\dot{\mathbf{d}}\mathbf{n}]}{cr^2}\,. \tag{10}$$

We note than one of the terms here decreases with r as $1/r$ and the other as $1/r^2$.

Next, we substitute potentials (6) in the expression for the scalar potential gradient to obtain

$$\begin{aligned}-\boldsymbol{\nabla}\varphi_{\rm d}&=-\frac{\boldsymbol{\nabla}\,(\mathbf{nd})}{r^2}+\frac{2\mathbf{n}\,(\mathbf{nd})}{r^3}\,,\\-\boldsymbol{\nabla}\varphi_{\rm rad}&=-\frac{\boldsymbol{\nabla}(\mathbf{n}\dot{\mathbf{d}})}{cr}+\frac{\mathbf{n}\,(\mathbf{n}\dot{\mathbf{d}})}{cr^2}\,.\end{aligned} \tag{11}$$

Using the vector analysis identity $\boldsymbol{\nabla}(\mathbf{ab})=(\mathbf{a}\boldsymbol{\nabla})\,\mathbf{b}+\big[\mathbf{a}[\boldsymbol{\nabla}\mathbf{b}]\big]+(\mathbf{b}\boldsymbol{\nabla})\,\mathbf{a}+\big[\mathbf{b}[\boldsymbol{\nabla}\mathbf{a}]\big]$ [4], we write the gradients of the scalar products in Eqns (11) as

$$\begin{aligned}\boldsymbol{\nabla}(\mathbf{nd})&=-\frac{\dot{\mathbf{d}}}{c}-\frac{1}{c}\,\big[[\dot{\mathbf{d}}\mathbf{n}]\,\mathbf{n}\big]+\frac{\mathbf{d}-\mathbf{n}(\mathbf{dn})}{r}\,,\\\boldsymbol{\nabla}(\mathbf{n}\dot{\mathbf{d}})&=-\frac{\ddot{\mathbf{d}}}{c}-\frac{1}{c}\,\big[[\ddot{\mathbf{d}}\mathbf{n}]\,\mathbf{n}\big]+\frac{\dot{\mathbf{d}}-\mathbf{n}(\dot{\mathbf{d}}\mathbf{n})}{r}\,.\end{aligned} \tag{12}$$

With Eqn (12) substituted in Eqn (11), the potential gradients can be written as

$$\begin{aligned}-\boldsymbol{\nabla}\varphi_{\rm d}&=\frac{\dot{\mathbf{d}}}{cr^2}+\frac{\big[[\dot{\mathbf{d}}\mathbf{n}]\,\mathbf{n}\big]}{cr^2}-\frac{\mathbf{d}}{r^3}+3\,\frac{\mathbf{n}(\mathbf{dn})}{r^3}\,,\\-\boldsymbol{\nabla}\varphi_{\rm rad}&=\frac{\ddot{\mathbf{d}}}{c^2r}+\frac{\big[[\ddot{\mathbf{d}}\mathbf{n}]\,\mathbf{n}\big]}{c^2r}-\frac{\dot{\mathbf{d}}}{cr^2}+2\,\frac{\mathbf{n}(\dot{\mathbf{d}}\mathbf{n})}{cr^2}\,.\end{aligned} \tag{13}$$

Noting that $\varphi_{\rm m}=0$ and $\big[[\dot{\mathbf{d}}\mathbf{n}]\,\mathbf{n}\big]=-\dot{\mathbf{d}}+\mathbf{n}(\dot{\mathbf{d}}\mathbf{n})$, we express the scalar potential gradient as

$$\begin{aligned}-\boldsymbol{\nabla}\varphi=-\boldsymbol{\nabla}\varphi_{\rm d}-\boldsymbol{\nabla}\varphi_{\rm rad}&=\frac{\ddot{\mathbf{d}}}{c^2r}+\frac{\big[[\ddot{\mathbf{d}}\mathbf{n}]\,\mathbf{n}\big]}{c^2r}\\&+\frac{-\dot{\mathbf{d}}+3\mathbf{n}(\dot{\mathbf{d}}\mathbf{n})}{cr^2}+\frac{-\mathbf{d}+3\mathbf{n}(\mathbf{dn})}{r^3}\,.\end{aligned} \tag{14}$$

According to Eqn (8),

$$-\frac{\dot{\mathbf{A}}_{\rm rad}}{c}=-\frac{\ddot{\mathbf{d}}}{c^2r}\,, \tag{15}$$

which, when added to Eqn (14), yields the electric vector

$$\mathbf{E}=-\boldsymbol{\nabla}\varphi-\frac{\dot{\mathbf{A}}}{c}=\frac{\big[[\ddot{\mathbf{d}}\mathbf{n}]\,\mathbf{n}\big]}{c^2r}+\frac{-\dot{\mathbf{d}}+3\mathbf{n}(\dot{\mathbf{d}}\mathbf{n})}{cr^2}+\frac{-\mathbf{d}+3\mathbf{n}(\mathbf{dn})}{r^3}\,, \tag{16}$$

with the terms decreasing with distance as $1/r$, $1/r^2$, and $1/r^3$.

Equations (10) and (16) determine the magnetic and electric fields generated by the charge and currents in region V at distances larger than the size of the region. Because the fields differ in the rate of decrease with the distance from V, the electric and magnetic fields can be expressed as the sum of two components:

$$\begin{aligned}\mathbf{E}(\mathbf{r},t)&=\mathbf{E}_{\rm F}(\mathbf{r},t)+\mathbf{E}_{\rm N}(\mathbf{r},t)\,,\\\mathbf{B}(\mathbf{r},t)&=\mathbf{B}_{\rm F}(\mathbf{r},t)+\mathbf{B}_{\rm N}(\mathbf{r},t)\,,\end{aligned} \tag{17}$$

where the electric and magnetic fields

$$\mathbf{E}_{\rm F}(\mathbf{r},t)=\frac{\big[[\ddot{\mathbf{d}}\mathbf{n}]\,\mathbf{n}\big]}{c^2r}\,,\quad\mathbf{B}_{\rm F}(\mathbf{r},t)=\frac{[\ddot{\mathbf{d}}\mathbf{n}]}{c^2r} \tag{18}$$

that decrease as $1/r$ are called the far fields, and their counterparts

$$\begin{aligned}\mathbf{E}_{\rm N}(\mathbf{r},t)&=\frac{-\dot{\mathbf{d}}+3\mathbf{n}(\dot{\mathbf{d}}\mathbf{n})}{cr^2}+\frac{-\mathbf{d}+3\mathbf{n}(\mathbf{dn})}{r^3}\,,\\\mathbf{B}_{\rm N}(\mathbf{r},t)&=\frac{[\dot{\mathbf{d}}\mathbf{n}]}{cr^2}\,,\end{aligned} \tag{19}$$

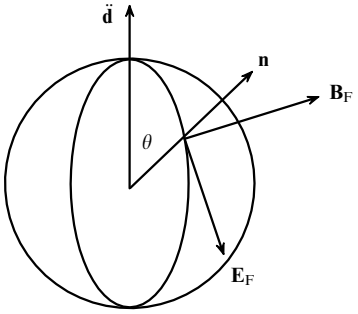

Figure 4. Illustration of how the far-field vector and the unit vector **n** are arranged with respect to each other.

decrease faster than $1/r$ and are called the near fields. These are precisely the near field mentioned in the Introduction in qualitatively explaining the higher resolving power of near-field microscopes compared with conventional optical microscopes. The far field is proportional to the second derivative of the system dipole moment. The $1/r^2$ part of the near field is due to the first derivative and vanishes in the static case. The $1/r^3$ electric dipole field does not vanish even in the static ($\dot{\mathbf{d}} = 0$) case. As we see in what follows, it is the alternating $1/r^3$ field that crucially determines the high resolving power of the SNOM.

We next find which fields cause the flow of electrons from the region V and are therefore responsible for the radiation from the tip of the needle. The far-field vectors $\mathbf{E}_\mathrm{F}(\mathbf{r}, t)$ and $\mathbf{B}_\mathrm{F}(\mathbf{r}, t)$ and the unit vector **n** constitute a right-handed triple of pairwise orthogonal vectors as shown in Fig. 4.

The Poynting vector of the far field has the form

$$\mathbf{S}(\mathbf{r}, t) = \frac{c}{4\pi}\,[\mathbf{E}_\mathrm{F}\mathbf{B}_\mathrm{F}] = \frac{c}{4\pi}\,\mathbf{n}\mathbf{B}_\mathrm{F}^2 = \mathbf{n}\,\frac{c}{4\pi}\,\frac{|\ddot{\mathbf{d}}|^2}{c^4 r^2}\,\sin^2\theta\,, \qquad (20)$$

which, when used to calculate the energy flux through a sphere around L, yields the well-known formula

$$I = \oint_\sigma (\mathbf{S}\,\mathrm{d}\boldsymbol{\sigma}) = \frac{|\ddot{\mathbf{d}}|^2}{4\pi c^3 r^2}\int_0^{2\pi} r\,\mathrm{d}\alpha \int_{-1}^{1} r\sin^2\theta\,\mathrm{d}\cos\theta = \frac{2|\ddot{\mathbf{d}}|^2}{3c^3}. \qquad (21)$$

The far field is the light that emanates from the needle. This radiation forms the image in the usual microscope and plays the role of beams in geometric optics. The far field does not allow overcoming the diffraction limit, which restricts the resolution of the usual microscope. The high resolution of SNOMs is due to the near field.

Because the electric and magnetic vectors of the near field decrease at least as $1/r^2$, it follows that the Poynting vector of the field decreases as $1/r^4$, and hence the integral over the surface surrounding region V tends to zero as $1/r^2$ with the distance from this region. This means that the near field does not take part in energy transfer from the region V. However, it plays a major role in exciting molecules near the SNOM probe.

To see that this is indeed the case, we compare the magnitudes of the electric vectors of the near and far fields in the near zone, that is, near the probe. Because

$$\frac{\dot{d}}{c} \propto \frac{\omega}{c}\,d = \frac{2\pi}{\lambda}\,d\,, \quad \frac{\ddot{d}}{c^2} \propto \left(\frac{\omega}{c}\right)^2 d = \left(\frac{2\pi}{\lambda}\right)^2 d, \qquad (22)$$

they are easily estimated to be

$$E_\mathrm{F} \propto \left(\frac{2\pi}{\lambda}\right)^2 \frac{d}{r}\,, \quad E_\mathrm{N} \propto \left(\frac{2\pi}{\lambda}\right)\frac{d}{r^2} + \frac{d}{r^3} \cong \frac{d}{r^3}\,. \qquad (23)$$

Noting the near-zone inequality $\lambda \gg r$, we see that the near field is substantially less than the far field in the near zone:

$$\frac{E_\mathrm{N}}{E_\mathrm{F}} \propto \frac{\lambda^2}{4\pi^2 r^2} \gg 1\,. \qquad (24)$$

It follows from Eqn (23) that the electric field in the near zone (that is, the near field) is in fact the field of a dipole oscillating at an optical frequency.

5. How are nanoobjects resolved in the microscope?

The common geometric-optics-based microscope uses the light propagating from the object (i.e., the far field) to form the image. The electric field of this light cannot be localized in a spatial region of a size less than the photon wavelength. The simplest way to show this is to use the uncertainty relation $px > h$ for the position and momentum of a photon, which, in view of $p = \hbar k = h/\lambda$, yields the well-known resolution condition

$$\frac{x}{\lambda} > 1 \qquad (25)$$

of conventional microscopy. Although this condition is derived using the Heisenberg uncertainty relation, it does not contain the Planck constant and is therefore nonquantum and equally well applicable to the classical light of geometric optics. The near-field microscope presents a totally different situation.

We return to Fig. 1, in which the probe is located at the distance from the surface of the sample less than its emitted wavelength. According to Eqn (25), the spot of light coming from the probe has a diameter not less than the wavelength, and hence, as can be seen from Fig. 1, covers a large number of molecules. We consider the absorption coefficient for a molecule excited by the electromagnetic field. The rate of excitation of a molecule by light is given by

$$k = 2\left(\frac{\mathbf{pE}}{\hbar}\right)^2 \frac{\gamma}{\Delta^2 + \gamma^2} \qquad (26)$$

(see, e.g., Eqn (7.42) in book [5]). Here, **p** is the dipole moment of the molecular transition, **E** is the vector of the electric field strength acting on the molecule, Δ is the difference between the frequency of the radiation from the probe and the resonance frequency of the molecule, and 2γ is the absorption line half-width of the molecule. The total electric field consists of a near field and a far field, i.e., $\mathbf{E} = \mathbf{E}_\mathrm{F} + \mathbf{E}_\mathrm{N}$. Because the near field decreases as $1/r^3$, it is essentially zero for molecules in the far zone, and hence $\mathbf{E} \cong \mathbf{E}_\mathrm{F}$ and the absorption coefficient for molecules at the periphery of the lightspot is given by

$$k_\mathrm{F} = 2\left(\frac{\mathbf{pE}_\mathrm{F}}{\hbar}\right)^2 \frac{\gamma}{\Delta^2 + \gamma^2}\,. \qquad (27)$$

In the near zone, i e., in the center of the light spot, besides a large increase in the magnitude of the far field, the near field is

added to it, whose strength is by Eqn (24) much larger than that of the far field in the near zone, i.e., $\mathbf{E}_N \gg \mathbf{E}_F$. The light absorption coefficient of a molecule in the near zone can therefore be expressed as

$$k_N = 2\left(\frac{\mathbf{p}(\mathbf{E}_N + \mathbf{E}_F)}{\hbar}\right)^2 \frac{\gamma}{\Delta^2 + \gamma^2} \gg k_F\,. \tag{28}$$

It then follows that in the near zone, with a spatial size less than the radiation wavelength, molecules absorb electromagnetic radiation much more effectively than their far zone counterparts. On the other hand, the higher the absorption is, the stronger the fluorescence of light-excited molecules. Therefore, in a setup with substrate molecules excited by a probe, the photomultiplier shown in Fig. 1 detects fluorescence only from molecules in the near zone, not from those in the far zone, even though all of them are covered by the light spot as seen in Fig. 1. It is for this reason that the resolving power of the SNOM is tens of times higher than that of conventional optical microscopes. Actual SNOMs have a spatial resolution about $\lambda/40$.

Acknowledgements. I thank N A Popov and B L Voronov for their critical reading of the manuscript. This work was supported by the Russian Foundation for Basic Research (grant Nos 08-07-00371, 07-02-00181, and 07-02-00547).

References

1. Binning G et al. *Phys. Rev. Lett.* **49** 57 (1982)
2. Pohl D W, Denk W, Lanz M *Appl. Phys. Lett.* **44** 651 (1984)
3. Landau L D, Lifshitz E M *Teoriya Polya* (The Classical Theory of Fields) (Moscow: Fizmatgiz, 1962) [Translated into English (Oxford: Pergamon Press, 1983)]
4. Tamm I E *Osnovy Teorii Elektrichestva* (Fundamentals of the Theory of Electricity) (Moscow: Nauka, 1966) [Translated into English (Moscow: Mir Publ., 1979)]
5. Osad'ko I S *Selektivnaya Spektroskopiya Odinochnykh Molekul* (Selective Spectroscopy of Single Molecules) (Moscow: Fizmatlit, 2000) [Translated into English (Berlin: Springer, 2003)]